Graefe's Arch Clin Exp Ophthalmol (1995)
233:123–130

CLINICAL INVESTIGATION

Ivo H.M. van Stokkum
George N. Lambrou
Tom J.T.P. van den Berg

Hemodynamic parameter estimation from ocular fluorescein angiograms

Received: 16 February 1994
Revised version received:
12 September 1994
Accepted: 16 September 1994

I.H.M. van Stokkum (✉)
Faculty of Physics and Astronomy,
Free University, De Boelelaan 1081,
1081 HV Amsterdam,
The Netherlands
FAX: (+31) 20–4447899

G.N. Lambrou · T.J.T.P. van den Berg
Laboratory of Medical Physics and
Informatics, AMC, Meibergdreef 15,
1105 AZ Amsterdam,
The Netherlands

Abstract ● Background: A method is proposed for parameterizing choroidal blood flow from fluorescein angiograms. ● Methods: After digitizing and aligning the angiographic sequence, the intensity build-up curves of fluorescence are analysed per pixel (approx. 10 μm in fundo). Two models are compared. A one-compartment model predicts an exponential build-up curve, from which the following parameters are estimated: maximum fluorescence, dye appearance time and local perfusion rate (reciprocal of the time constant of the exponential). To account for the contribution of the systemic circulation to the shape of the build-up curve, a two-compartment model is used which predicts a bi-exponential curve. ● Results: Introduction of the second (systemic) compartment resulted in a significant improvement of fit in 37 of 48 patients studied. The rate constants of the systemic compartment found were mainly in the range of 0.30–1.00 s^{-1}. ● Conclusion: For the individual patient, the local perfusion rates may vary strongly, with lower perfusion rates possibly being of prognostic value for ocular diseases such as glaucoma or diabetic retinopathy.

Introduction

The choroidal circulation makes an important contribution to the nourishment of the outer retina and of the optic nerve head. Its role in the pathogenesis of retinal disorders, or in potentially ischemic ocular conditions like glaucoma, has long been postulated [1, 4, 5, 7, 11] but is still an object of controversy. One of the reasons is the lack of a clinically acceptable technique for parameterizing choroidal blood flow.

Since the advent of fluorescein angiography it has been possible to visualize certain aspects of the retinal and choroidal circulations. The routine interpretation of angiograms is still subjective and purely qualitative, but a substantial number of studies have aimed at some form of quantification of retinal blood flow in vivo [2]. This is not the case, however, for the choroidal circulation. Only very recently have some attempts been made to derive hemodynamic parameters from fluorescence intensity curves obtained from angiographic sequences [14, 17, 19]. These attempts, highly computation intensive, have been made possible by the popularization of image-processing facilities.

In a previous publication [17], we sketched an approach to the analysis of angiographic fluorescence-intensity curves, based on a simple model of the choroidal filling. This first approach was a variant of the dye dilution curve analysis, assuming the entrance of the dye in the ocular vessels to be a step function, and the choroidal vasculature to behave like a single compartment. The purpose of the present paper is to refine the approach, by taking into account the conditions of ocular delivery of the dye, and to estimate the choroidal perfusion rate from routine clinical angiograms.

Materials and methods

Experimental

The data to be analysed were extracted from routine clinical angiograms recorded on black-and-white negative films. The procedure for obtaining such angiograms is the following: After pharmaceutical dilation of the pupil and cannulation of a peripheral vein (usually the antecubital), the patient is seated in front of a fundus camera which incorporates a coaxial flash tube, a timer and an adequate set of filters. The fluorescent dye (in this case 3 ml of 25% sodium fluorescein) is then injected in the vein canula as fast as possible, and at the same time the timer of the camera is started. The time necessary for the dye to reach the eye through the systemic venous circulation, right heart, pulmonary circulation, left heart, and systemic arterial tree ("arm-retina time") is 8–12 s. Six seconds after the injection, i.e. before the dye has reached the eye, photographs start being taken at the maximum rate of flash delivery (recharge), which is of the order of 0.75–1.0 s, depending on the camera. Photographs are taken at that rate until the end of the film. As some of the first frames of the film are used for recording patient data, white light and red-free light photographs of the fundus, approximately twenty frames are recorded per angiogram. The camera incorporates non-overlapping filters, positioned in front of the flash tube and of the film, ensuring that during angiography only the light emitted by the dye is recorded on the film. Thus, the first frames in the sequence (before arrival of the dye) are unexposed and the last frames, after the dye has penetrated all vessels, are nearly identical. Each frame is time-stamped by the camera. In routine clinical practice, paper prints made from the negatives are assessed by eye. For the present study, the central part of each negative (corresponding to an area approximately $25° \times 25°$ in the fundus) was digitized as an 8-bit, 256×256 pixel image, using a black-and-white real-time frame grabber (Synaps-MAPP, Les Ulis, France) in a PC-AT type computer. A limited number of successive frames (between 10 and 21) were digitized from each angiogram, starting a few seconds before arrival of the dye and, whenever possible, extending a few seconds after the emitted intensity had reached its maximum value. Intensity build-up curves were extracted for each pixel over the whole sequence of digitized frames. The frames of each sequence were aligned manually relative to a reference frame from the middle of the sequence. In a few cases the alignment was improved with the help of an image-processing algorithm which matched local regions of interest in successive images [12]. From these matches the optimal geometric transformation is found.

The research followed the tenets of the declaration of Helsinki. Informed consent was obtained from all patients prior to the study.

Theoretical

The simple model used in the preliminary studies [17, 18] describes the concentration of fluorescein $c(t)$ at a given site of the fundus by a first-order differential equation. The differential equation of the one-compartment model [8] is

$$\frac{\mathrm{d}}{\mathrm{d}t} c_1^I(t) = -k_1 c_1^I(t) + i(t) \tag{1}$$

where k_1 is a rate constant (reciprocal of time constant) describing the rate of filling with fluorescein and $i(t)$ is the speed of delivery of dye by the arteries to the fundus site per unit volume. The subscript 1 indicates compartment 1, whereas the superscript I indicates the one-compartment model. With zero initial conditions and $i(t)$ a step input, the solution of Eq. 1 is given by

$$c_1^I(t) = c_{1,\infty}(1 - e^{-k_1 t}) \tag{2}$$

where $c_{1,\infty}$ is the steady-state concentration resulting from the step input.

The next simplest model describes the concentration of fluorescein in a given site of the fundus with two coupled first-order differential equations. Thereby compartment 2 represents the systemic circulation from the injection site to the arteries which supplies the ocular compartment 1. The differential equations of the two-compartment model are

$$\frac{\mathrm{d}}{\mathrm{d}t} c_2^{II}(t) = -k_2 c_2^{II}(t) + i(t)$$

$$\frac{\mathrm{d}}{\mathrm{d}t} c_1^{II}(t) = -k_1 c_1^{II}(t) + k_{12} c_2^{II}(t) \tag{3}$$

k_2 is a rate constant describing the rate of filling with fluorescein of compartment 2, $k_{12} c_2^{II}(t)$ is the speed of delivery of dye by the arteries to the fundus site per unit volume and $i(t)$ represents injection of dye in a peripheral vein. With zero initial conditions and $i(t)$ a step input, we have the solution

$$c_2^{II}(t) = c_{2,\infty}(1 - e^{-k_2 t}) \tag{4}$$

$$c_1^{II}(t) = c_{1,\infty}\left(1 - \frac{k_1}{k_1 - k_2} e^{-k_2 t} + \frac{k_2}{k_1 - k_2} e^{-k_1 t}\right) \tag{5}$$

$c_{1,\infty}$ and $c_{2,\infty}$ are the steady-state concentrations resulting from the step input, $c_{2,\infty} = c_{1,\infty} k_1 / k_{12}$. In case $k_1 = k_2$ we find $c_1^{II}(t) = c_{1,\infty}(1 - e^{-k_1 t} - k_1 t e^{-k_1 t})$.

In routine angiography the fluorescence intensity is measured as a function of fundus position at n sequential time instants, typically $n = 20$. We assume this intensity to be proportional to $c_1(t)$, the fluorescein concentration in a fundus site. We also assume this intensity to be proportional to the density of the film $f(t)$, which is the quantity actually measured. These assumptions are valid within given ranges of dye concentration and film exposure respectively (G.N. Lambrou, A.A.J. Jonker, A. van Baren, T.J.T.P. van den Berg, unpublished work).

Another assumption in the design of the models is that the fluorescence emitted from fundus sites with no dominant retinal features (macula, retinal vessels) originates essentially from the choriocapillaris level. Alternative sources of fluorescence might be (a) dye in the more superficial (retinal) microcirculation, and (b) in the deeper (large choroidal vessel) layers. This point is discussed further on.

Because the number of time points is small, we cannot estimate the systemic dynamics parameter k_2 from each fundus site separately. We therefore decided to link k_2 across the fundus. In practice a grid of m fundus sites, typically $m = 64$, was used.

The one-compartment model function for the film density $f(t)$, which is assumed to be proportional to dye concentration in a fundus site, contains three parameters which need to be estimated. Parameter d represents the steady-state level of the film density, t_0 represents the delay time from the moment of injection. Because a rate constant is by definition positive we fitted its logarithm. Thus we arrived at the model function

$$f^I(t) = d(1 - e^{-k_1 t}) \quad t = t_j - t_0 > 0 \quad j = 1, n \tag{6}$$

The parameterization of Eq. 5 requires the extra systemic rate parameter k_2 (which we again forced to be positive by fitting its logarithm), which gives the two-compartment model function to be fitted:

$$f^{II}(t) = d\left(1 - \frac{k_1}{k_1 - k_2} e^{-k_2 t} + \frac{k_2}{k_1 - k_2} e^{-k_1 t}\right)$$

$$t = t_j - t_0 > 0 \quad j = 1, n \tag{7}$$

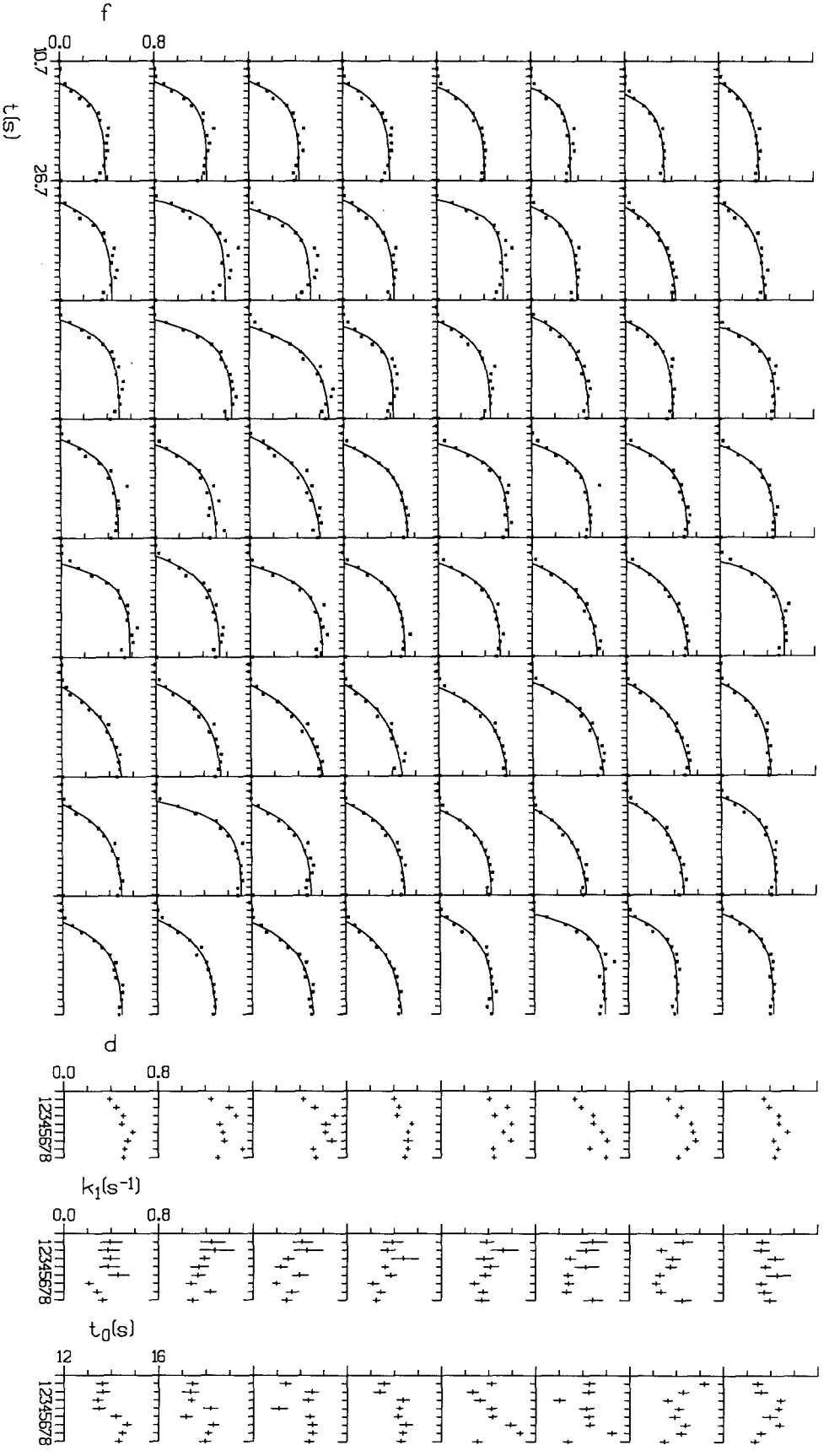

Fig. 1 Overview of fit results of density curves (of $n=17$ points) from patient L.G.M. using the one-compartment model. Fitted curves are shown at the 8×8 fundus points. In the three rightmost columns, respectively, d, k_1 and t_0 belonging to a row of fundus sites are drawn. The plus signs indicate the estimates, with the vertical bar indicating the approximate standard error in the parameters $\pm\sigma_d$ etc.

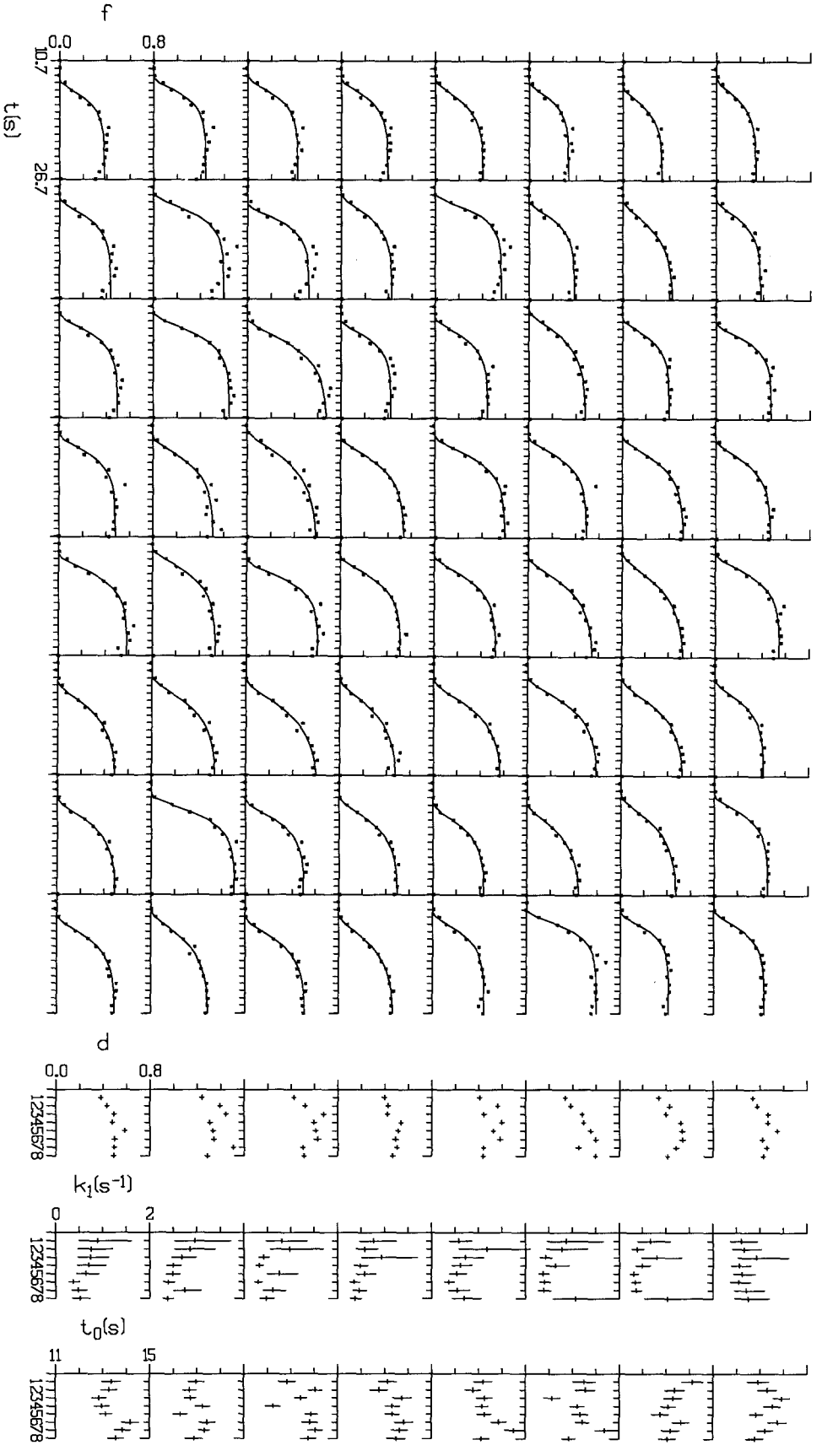

Fig. 2 Overview of fit results of the same 8×8 density curves from patient L.G.M. using the two-compartment model. Layout as in Fig. 1

The parameter estimation procedures were implemented in Fortran 77 using mathematical and statistical routines from International Mathematical and Statistical Libraries, (Houston Tex). To speed up the nonlinear least squares (NLLS) fitting of the two-compartment model we eliminated the linear parameters with the help of the variable projection method [9, 13, 20, 23]. Typical computation times on a SUN SLC for an 8×8 grid of fundus sites were 20 and 200 s for, respectively, one- and two-compartment fitting.

Results

We will present results from one patient (L.G.M.) in detail and summarize the results from a population study of 48 patients. These patients suffered either from glaucoma (primary open angle or normal pressure) or from diabetic retinopathy. The relation between the estimated parameters and the clinical status of these patients is beyond the scope of this paper and is still under investigation. In our preliminary study [17], each of the 256×256 density curves was analysed independently using Eq. 6, after linearization of the parameters [6]. If, however, the extra parameter (k_2) is to be introduced in the model, all the time curves have to be fitted simultaneously. Clearly, a simultaneous fit of all $256 \times 256 \times 2 + 1$ parameters is not feasible. Therefore k_2 is estimated from a regularly spaced 8×8 selection, and k_2 is fixed when fitting Eq. 7 for all 256×256 density curves.

Thus we can estimate 256×256 parameters d, k_1, t_0 from a one-compartment model (Eq. 6) and from a two-compartment model (Eq. 7).

In Figs. 1 and 2 we see the results of fits of data obtained from patient L.G.M. at a grid of 8×8 distinct fundus sites (regularly distributed over the whole fundus area, as indicated by the squares in Figs. 3 and 4) with, respectively, the one- and two-compartment model. The improved alignment procedure was applied to these data. The global root-mean-square error σ (from the NLLS fit) decreases from 0.0320 to 0.0282 when the second compartment is added. When we define the relative improvement γ as $\gamma = (\sigma_I - \sigma_{II})/\sigma_I$ this amounts to 12%. Comparing Fig. 1 and Fig. 2, the improvement gained with the two-compartment model is visible in the onset of the density curve in many fundus sites. In the three rightmost columns, parameter estimates (respectively, d, k_1 and t_0) belonging to a row of fundus sites are drawn. The plus signs indicate the NLLS estimates, with the vertical bar indicating the error in the parameters, $\pm \sigma_d$ etc. Note that the differences between the t_0 and k_1 parameters of the one- and two-compartment model depend upon the extra parameter k_2. The uncertainty in the estimated parameters is small for the maximum density, but large for the rate and appearance time parameters (tens of percents relative error), as can be seen from the vertical bars in the first and the last two columns of Fig. 1 and Fig. 2. Introduction of the second compartment rate parameter of course increases these uncertainties.

We compared the two models for analysis of the angiograms of the patients described at the beginning of this section. Of 48 angiograms studied we found a relative improvement of the goodness of fit $\gamma \geq 5\%$ in 26 cases when the second compartment is introduced. The maximum improvement found was 17%. In 11 cases $1\% \leq \gamma \leq 5\%$, and in 11 cases $0\% \leq \gamma \leq 1\%$.

The rate constant of the global compartment (systemic circulation), k_2, could be reliably determined in 37 cases. It ranged from 0.12–1.66 s^{-1}, but in 31 cases it was in the interval of 0.30–1.00 s^{-1}.

Figures 3 and 4 depict grey-scale maps of the parameters estimated for patient L.G.M. using respectively, the one and two compartment models. The grey scale is designed with the convention that darker indicates "worse" circulation (i.e. lower maximal density, lower rate of perfusion and later appearance time) whereas lighter indicates "better" circulation. The squares indicate the grid of 8×8 fundus sites used with Fig. 1 and Fig. 2. For instance, the site row 7, column 7 corresponds to an artery, with a large value of d. The maximum density maps (Figs. 3a, 4a) are not very different from a late angiographic frame. In the rate maps (Figs. 3b, 4b) a lower perfusion rate is visible in the temporal half of the choriocapillaris. Comparing the two maps, some differences can be seen. Figure 4b represents a larger dynamic range of k_1 and provides a better contrast than Fig. 3b. With patient L.G.M. the local rate k_1 varied between 0.29 and 0.92 s^{-1}, whereas the global rate k_2 was estimated to be about 0.64 s^{-1}. Finally, the t_0 maps (Figs. 3c, 4c) show a highly delayed appearance in the territory temporal to the optic nerve head. Comparing the two maps, this delay appears to be closer to the t_0 of the veins in Fig. 4c than in Fig. 3c.

Discussion

The interpretation of fundus fluorescence build-up curves requires some assumptions about the origin of the fluorescent light, given the fact that complex three-dimensional angioarchitecture is projected on two-dimensional angiographic frames.

In a normal fundus, one can roughly distinguish three circulatory layers. The (most superficial) retinal circulation is the most striking feature of the angiogram because of the high contrast and crisp detail of its vessels. It is evident that fluorescence recorded over such vascular features originates predominantly from intravascular dye. The retinal microcirculation, however, makes a limited contribution to fundus fluorescence because of its small volume and because the blood-retina barrier precludes dye-leakage. This is supported by two types of angiographic evidence: In areas of delayed, masked or inexistent choroidal filling (e.g. with targeted

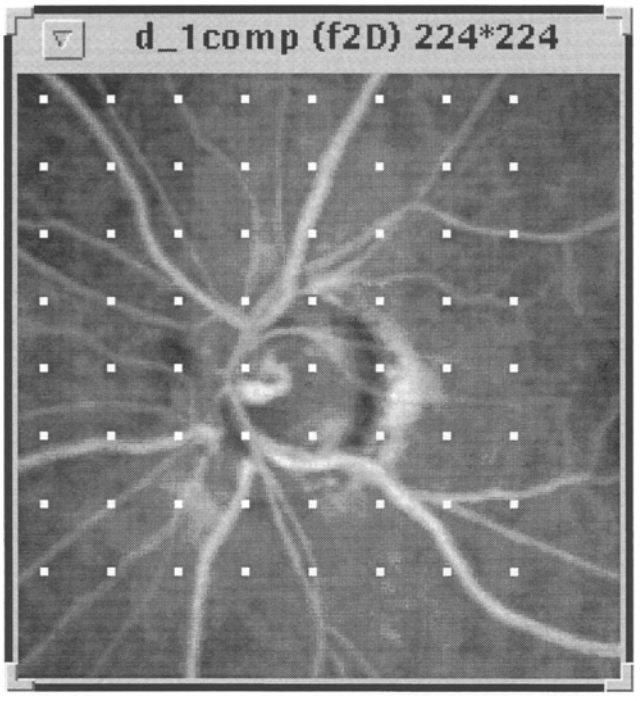

a

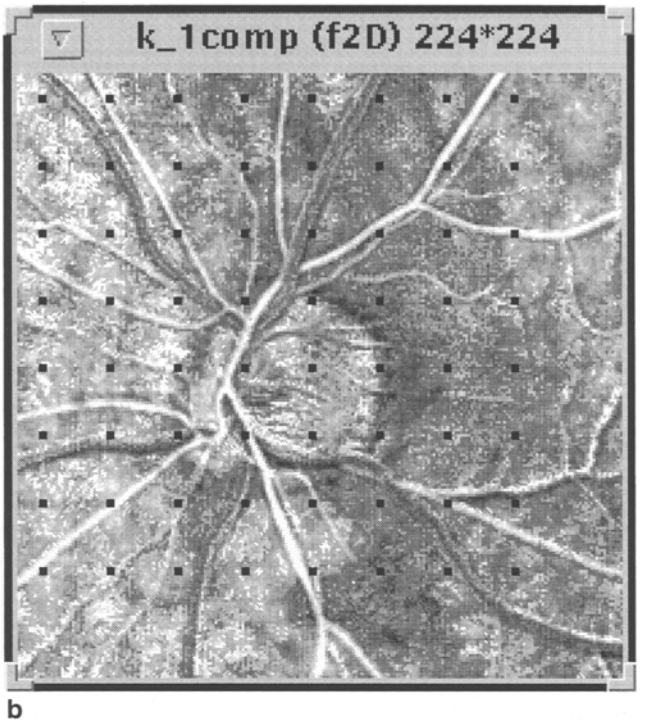

b

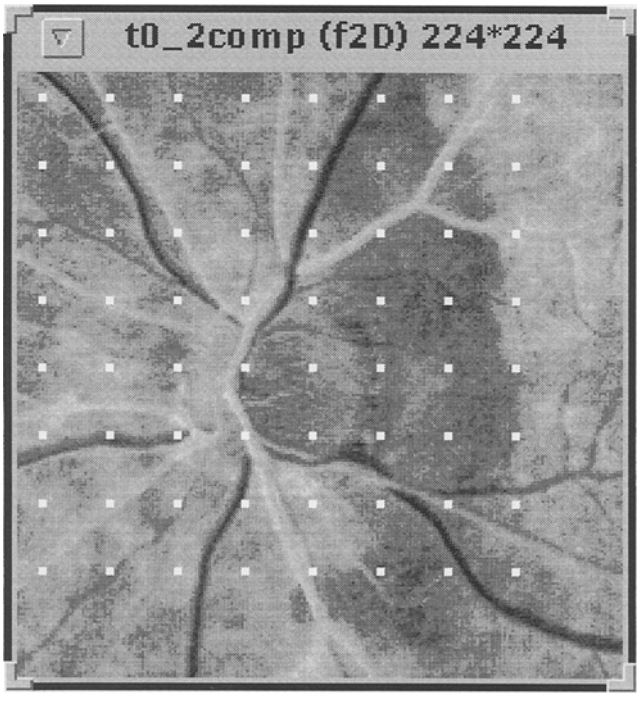

c

Fig. 3a–c Grey-scale maps (224 × 224 pixels) of estimated parameters from patient L.G.M. using the one-compartment model. The squares indicate the positions of the grid used in Figs. 1 and 2. **a** Maximum density d; **b** local perfusion rate k_1; **c** Delay time t_0. *Extrema* (respectively, black and white): **a** 0.278 and 0.905, **b** 0.118 and 0.572 s^{-1}, **c** 16.36 and 12.54 s

dye delivery), smaller retinal vessels can be resolved but neither the actual capillary network nor any homogeneous capillary fluorescence is visible. In contrast, when there is a breakdown of the blood-retina barrier, the leakage of dye in the retinal tissue results in a strong fluorescent spot obscuring the deeper (choroidal) layers.

So, in the absence of such distinctive retinal features, the fluorescent light originates from the choroidal level. Absorption by hemoglobin and fluorescein (intravascular or extravasated) restricts the penetration depth of the exciter light to ca. 30 μm (G.N. Lambrou, A.A.J. Jonker, A. van Baren, T.J.T.P. van den Berg, unpublished work), limiting strongly the contribution of the large choroidal vessels to fundus fluorescence. Only in the presence of an exceptionally thin or atrophic choriocapillaris do these vessels become visible in the early angiographic frames.

The two-compartment model allows separation of hemodynamic properties of systemic and choroidal circulation, thus giving a better basis for usage of this analysis. On the other hand, the quality of fit of the one-compartment model is already quite good (Figs. 1, 3), so this model is apt for not too demanding applications. A clear improvement in goodness of fit with a two-compartment model is present in 26 of 48 cases, while a moderate improvement is found in 11 of 48. It is natural that addition of the extra parameter, the rate constant of the second compartment, never causes deterioration of the NLLS fit. The success of the two-compartment model depends upon the quality of the data (signal-to-noise ratio) and upon both the number of data points

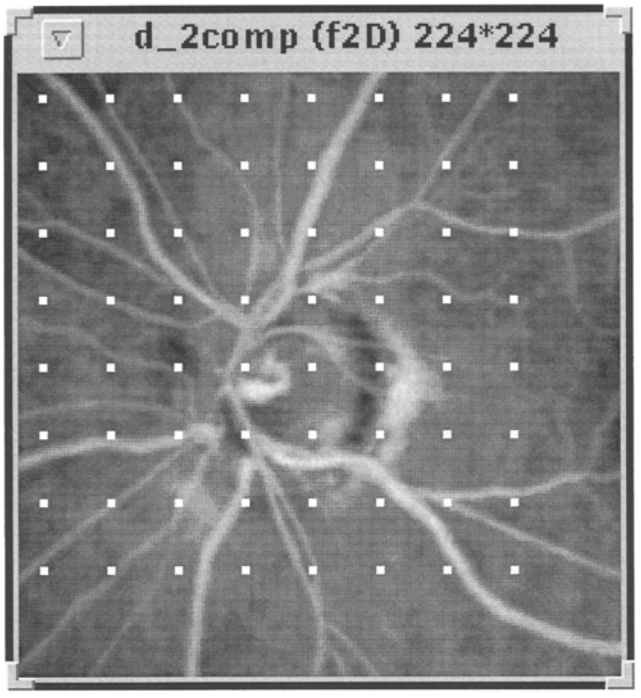

a

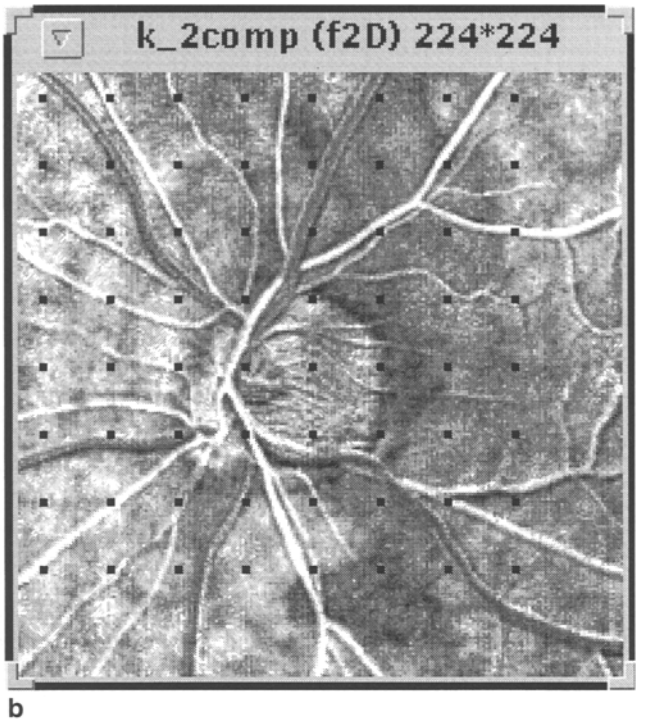

b

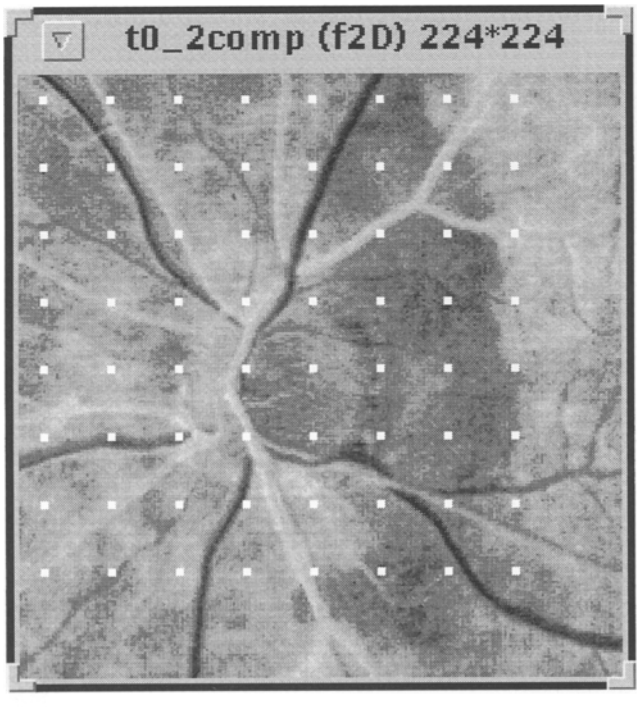

c

Fig. 4a–c Grey-scale maps of estimated parameters from patient L.G.M. using the two-compartment model. Layout as in Fig. 3. *Extrema*: **a** 0.278 and 0.905 (as in Fig. 3a), **b** 0.156 and 0.934 s^{-1}, **c** 15.43 and 11.61 s. Note that the difference between these extrema is the same as in Fig. 3c

taken during the rising phase of the density curve and the availability of data points before and after the rising phase.

With respect to the quality of the data, we have made special efforts to align the photographs correctly, manually or automatically [12], in order to improve the fit of the density build-up curves, since shifts of a few pixels across vessel edges cause large outliers. It is remarkable that about one image per second is sufficient for fitting such a complicated model with rate constants of about 0.7 s^{-1}. It is to be expected that higher temporal resolution will enable more accurate estimation of the parameters. With higher temporal resolution the cyclic variation that may be caused by the cardiac cycle [14] (G.N. Lambrou, P.R. Preußner, T.J.T.P. van den Berg, G. Richard, E.L. Greve, unpublished work), might have to be incorporated into the model. This could be a source of error.

The grey-scale maps of parameters (Figs. 3, 4) present a concise summary of the angiographic sequence, which can be interpreted quantitatively. In particular, the information presented in the perfusion rate maps (Figs. 3b, 4b) is very hard to extract by eye from an angiographic sequence, even with experienced examiners. When angiograms are interpreted subjectively, prominent features such as retinal microaneurysms or choroidal watershed zones are immediately recognized and characterized by the examiner, but an assessment of choroidal perfusion requires very careful scrutiny of the whole sequence and an important amount of mental abstraction, if one wants to separate factors leading to

the observed fluorescence patterns. Transient choroidal hypofluorescence, for instance, may be due to late dye appearance, to slow filling, or to both. By separating the two phenomena, the method presented here reduces the number of images to be assessed to three (the three parameter maps instead of the whole angiographic sequence), facilitates the qualitative interpretation of the choroidal circulation, and permits parameterization of the choriocapillaris perfusion.

Based on the assumption that the prelaminar region of the optic nerve head shares a common arterial supply with the peripapillary choroid [10], analysis of the perfusion rates of the latter may prove a useful tool for the prognostic assessment of glaucoma patients and ocular hypertensives. This expectation is enforced by the results of a previous investigation [16], as well as by literature data [15, 21, 22], indicating that the choroidal blood flow is reduced in normal-pressure glaucoma. This method could also prove useful in diabetic retinopathy, where neovascular proliferation depends on the degree of ischemia of the inner retina, more or less efficiently compensated by diffusion of oxygen and metabolites from the choriocapillaris [3]. Moreover, this method could be used to quantify the leakage of fluorescein (in terms of appearance time and rate of leakage) for follow-up and evaluation of treatment efficacy.

Acknowledgements The authors are grateful to Drs E.L. Greve and H.C. Geijssen for providing clinical angiograms of their patients. F. Temporelli, E. van Munster, F. Stiva and E. de Waal are thanked for programming assistance. M.D. in den Haak is thanked for help with the alignment of photographs. Dr F.C.A. Groen is thanked for critical reading of the text and helpful discussion.

References

1. Blumenthal M, Gitter KA, Best M, Galin MA (1970) Fluorescein angiography during induced ocular hypertension in man. Am J Ophthalmol 69:39–43
2. Bursell S-E, Clermont AC, Shiba T, King GL (1992) Evaluating retinal circulation using video fluorescein angiography in control and diabetic rats. Curr Eye Res 11:287–295
3. Buzney SM, Weiter JJ (1984) Pathogenesis of diabetic retinal angiopathy: proposed mechanisms and current research. Int Opthalmol Clin 24:1–12
4. Cristini G (1951) Common pathological basis of the nervous ocular systems in chronic glaucoma. Br J Ophthalmol 35:11
5. Dollery CT, Henkind P, Kohner EM, Paterson JW (1968) Effect of raised intraocular pressure on the retinal and choroidal circulation. Invest Ophthalmol 7:191–198
6. Foss SD (1969) A method of exponential curve fitting by numerical integration. Biometrics 25:815–821
7. Geijer C, Bill A (1979) Effects of raised intraocular pressure on retinal, prelaminar, laminar, and retrolaminar optic nerve blood flow in monkeys. Invest Ophthalmol Vis Sci 18:1030–1042
8. Godfrey K (1983) Compartmental models and their application. Academic Press, London
9. Golub GH, LeVeque RJ (1979) Extensions and uses of the variable projection algorithm for solving nonlinear least squares problems. Proc 1979 Army Numerical Analysis and Comp Conf, ARO Report 79 3:1–12
10. Hayreh SS (1978) Structure and blood supply of the optic nerve. In: Heilmann K, Richardson KT (eds) Glaucoma: conceptions of a disease. Thieme, Stuttgart, pp 78–96
11. Hayreh SS (1978) Pathogenesis of optic nerve damage and visual field defects. In: Heilmann K, Richardson KT (eds) Glaucoma: conceptions of a disease. Thieme, Stuttgart, pp 104–137
12. In den Haak MD, Spoelder HJW, Groen FCA (1992) Matching of images by using automatically selected landmarks. In: Dietz JLG (ed) Proceedings of Computer Science in the Netherlands 1992. Stichting Mathematisch Centrum, Amsterdam, pp 27–40
13. Kaufman L (1975) A variable projection method for solving separable nonlinear least squares problems. BIT 15:49–57
14. Klein GJ, Baumgartner RH, Flower RW (1990) An image processing approach to characterizing choroidal blood flow. Invest Ophthalmol Vis Sci 31:629–637
15. Laatikainen L (1971) Fluorescein angiographic studies of the peripapillary and perilimbal regions in simple, capsular and low-tension glaucoma. Acta Ophthalmol 111 [Suppl]: 9–83
16. Lambrou GN, Sindhunata P, Van den Berg TJTP, Geijssen HC, Vyborny P, Greve EL (1989) Ocular pulse measurements in low-tension glaucoma. In: Lambrou GN, Greve EL (eds) Ocular blood flow in glaucoma. Kugler & Ghedini, Amsterdam, pp 115–120
17. Lambrou GN, Van den Berg TJTP, Greve EL (1989) Vascular plerometry of the choroid. An approach to the quantification of choroidal blood flow using computer-assisted processing of fluorescein angiograms. In: Lambrou GN, Greve EL (eds) Ocular blood flow in glaucoma. Kugler & Ghedini, Amsterdam, pp 287–294
18. Lambrou GN, Van den Berg TJTP, Hayreh SS, Greve EL (1991) Automatic estimation of choriocapillaris blood flow parameters by image processing of fast fluorescein angiograms. (ARVO abstracts) Invest Ophthalmol Vis Sci 32 [Suppl]: 866
19. Prünte C, Niesel P (1988) Quantification of choroidal blood-flow parameters using indocyanine green videofluorescence angiography and statistical picture analysis. Graefe's Arch Clin Exp Ophthalmol 226:55–58
20. Seber GAF, Wild CJ (1989) Nonlinear regression. Wiley, New York
21. Spaeth GL (1977) The pathogenesis of optic nerve damage in glaucoma: contributions of fluorescein angiography. Grune & Stratton, New York
22. Ulrich WD, Ulrich A, Petzschmann Ä, Ulrich Ch (1988) Okuläre Autoregulation und ziliare Perfusionsdruck beim Niedrigdruckglaukom. Fol Ophthalmol 13:333–337
23. Van Stokkum IHM (1992) User note. Solving a separable nonlinear least squares problem: parameter estimation of time resolved spectra. IMSL/Directions 9 1:10–11